Design for Thermal Comfort in Passenger Vehicle Cabin

Ibrahim Reda[1], Essam E. Khalil[2], Taher M. Aboudeif[3], Ahmed El Degwy[4]

Abstract

Thermal comfort in a vehicle cabin can affect driver's and passengers' health, performance and comfort. Due to spatial and temporal variation of state variables and boundary conditions in the vehicle cabin, the heating, ventilating and air-conditioning (HVAC) system does not have to be designed to provide a uniform environment, especially because of individual differences regarding physiological and psychological response, clothing insulation, activity, air temperature and air movement preference, etc. The main objective of this research is to study the airflow regimes and thermal comfort in a vehicle cabin using computational fluid dynamics (CFD) software. For this purpose, CFD software from ANSYS Inc., called Fluent 17.2, is employed, in which the solar load model is embedded s2s (surface to surface) as a solar radiation model. The CFD modeling techniques solved the continuity, momentum and energy conservation equations in addition to standard k – ε model equations for turbulence closure. Meshing is processed around 4.0 million unstructured tetra-elements approximately. The performance of the air conditioning system is characterized by airflow regimes (air temperature, air velocity, relative humidity, PMV and PPD contours). The present work is focused on the effect of air terminal shape of the HVAC system. Two configurations are used in Case 1 and Case 2. Case 1 is the existing design of air terminals of the HVAC system of the selected car (Skoda Superb), with the air terminals in rectangular shape. In Case 2, they are in circular shape.

Keywords

CFD, Airflow regimes, Thermal comfort, PMV, PPD.

About the Authors

1 M.Sc. Student, Department of Mechanical Power, Faculty of Engineering, Cairo University.

2 Professor of Mechanical Power Engineering, Faculty of Engineering, Cairo University.

3,4 Assistant Professor of Mechanical Power Engineering, Faculty of Engineering, Cairo University.

Introduction

As vehicles become an indispensable part of everyday life, people spend 1-10 hours each day in vehicles [1]. Therefore the thermal comfort of passengers draws more and more attention. High levels of vehicle comfort are being increasingly demanded by users nowadays, creating a new challenge for climate control engineers. In the past, it typically took a year to develop and fully characterize the HVAC system for a new vehicle model using conventional physical testing methods. However, the use of computational fluid dynamics (CFD) simulators can dramatically reduce the time for development of automotive HVAC systems, contribute to improvement of their performance and provide better understanding of the underlying processes.

Thermal comfort not only affects the energy consumption of the HVAC system, but also is a key parameter for passenger health. It contributes to safe driving by reducing driver stress, avoiding windshield fogging and guaranteeing good visibility. Comfortable climate is usually defined as "the condition of mind that expresses satisfaction with the thermal environment" [2]. The human climate experience is essentially an interaction between six parameters: air temperature, mean radiant temperature, relative air movement, air humidity, activity level and thermal properties of clothing and seats. It is also possible to further divide the physical comfort sensation in two categories: local and whole body thermal comfort. The whole body value only consists of a mean value, while the local values take into consideration effects on different body parts individually.

Numerical Model Description

The car model chosen for the present analysis is Skoda Superb. The blueprints of its geometry can be easily found on the web. The geometry of the cabin was constructed using Solidworks v.17 software (*Figure 1*). The compartment was modeled as 1.5

m × 1.2 m × 3.0 m, x, y, z respectively. Further, several features were added to the model to make it ready to mesh in Fluent 17.2; four passengers were added to the model, and the interior volume of the vehicle cabin was estimated to be 2.6 m^3. The total glass surface area including the windshield and the side and rear glasses was estimated to be 3.2 m^2.

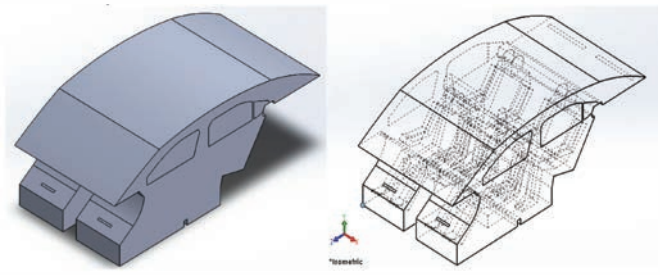

Figure 1: Vehicle cabin complex geometry (Solidworks v.17)

Figure 2 illustrates the computational model (ANSYS 17.2) of the cabin in Case 1 with 14 supply inlets and 2 return outlet air terminals. Four inlets are located on the front dashboard: one on the driver's left side (A_1), one on the front passenger's right side (A_2), and two in the center (B_1, B_2). Two inlets are located to maintain defrost (C_1, C_2) where the windshield meets the front dashboard. Two inlets are located to supply air to each side window (D_1, D_2), with another two inlets serving the rear passengers (G_1, G_2). The remaining four inlets are located in the leg space of the four passengers (E_1-E_4, F_1-F_4, H_1-H_4, and I_1-I_4). Two outlet vents (M_1) are located where the rear window meets the rear board of the passenger compartment [3].

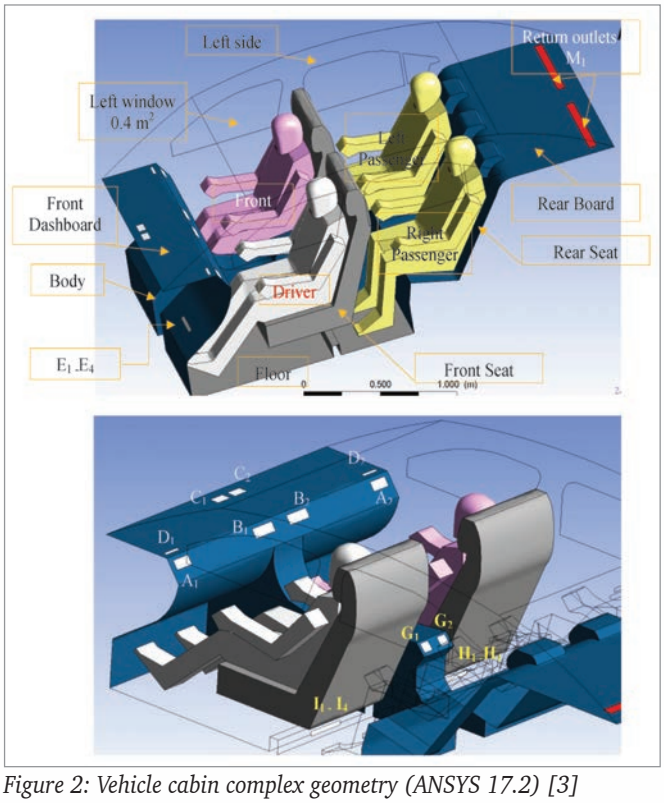

Figure 2: Vehicle cabin complex geometry (ANSYS 17.2) [3]

Case Studies

Case 1 Modeling

Configuration

Figure 3 shows the geometry of the cabin in Case 1, as already exists in the vehicle Skoda Superb. There are 14 supply (white) inlets, and 2 return (red) outlets. All the outlets are in rectangular shape.

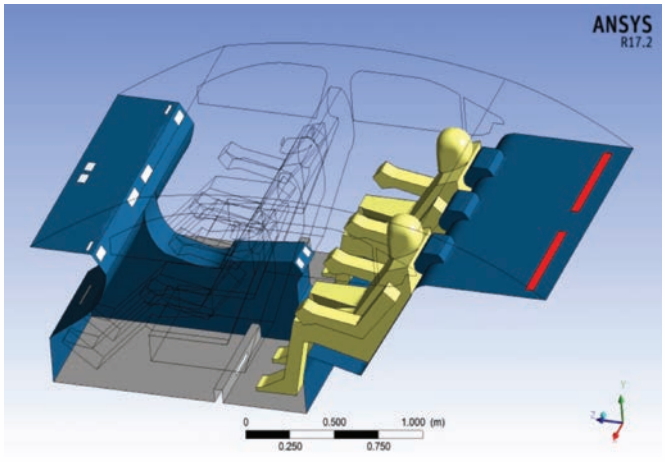

Figure 3: Geometrical configuration of Case 1

Boundary Conditions

Joo Hyun Moon et al. [4] considered inlet velocity as 3.27 m/s inside the compartment.

Han and Huang [5] suggested passenger thermal load to be considered as a heat flux of 80 W/m^2.

Using ASHRAE realistic method for calculating the direct and diffused solar irradiation on the earth's surface applied to Cairo (latitude 30.05°) at 13.00 hours on June 21 while the windshield is tilted 30° facing south (surface azimuth angle equals zero for maximum solar heat gain) and the altitude angle is 75°, solar irradiation of 970 W/m^2 is specified. The normal direct irradiation will be 880 W/m^2, and the diffused solar irradiation will be 110 W/m^2.

The emissivity for interior surfaces equals 0.95 [6], and for glass it equals 0.88 [7].

The properties of human body and materials are specified in *Table 1*.

Inlet temperature is 12°C.

Table 1: Properties of human body and materials [8]

	Material	Density [kg m^{-3}]	Specific heat [J kg^{-1} K^{-1}]	Thermal conductivity [W m^{-2} K^{-1}]
Windshield, rear, side glass	Glass	2529.58	754.04	1.1717
Body, dashboard, rear board	ABS plastic	996.35	1480.60	2.70
Seat	Polyurethane foam	70.00	1685.60	0.05
Floor	Carpet	1601.85	1485.38	0.2942
Driver	Skin	1000	3770	0.21

Case 2 Modeling

Configuration

Figure 4 shows the geometry of Case 2, which is planned for comparison of the vehicle cabin geometry. There are 14 supply (white) inlets, and 3 return (red) outlets, all in circular shape equal to the total area of the rectangular shape in the geometry of Case 1.

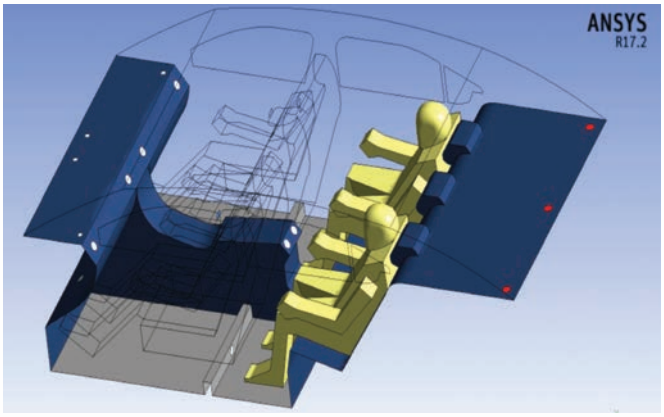

Figure 4: Geometrical configuration of Case 2

Boundary Conditions

All boundary conditions are copied from Case 1.

Results and Discussion

Temperature Contours

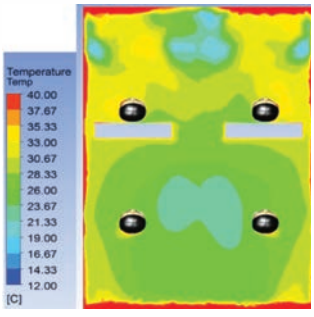

Figure 5: Temperature contour at horizontal plane (ZX) at Y=0.9 m (head level)

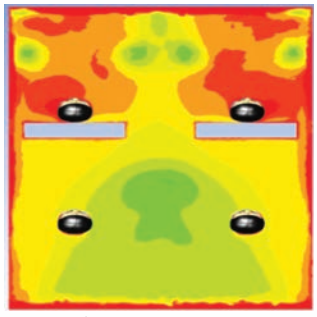

Figure 6: Temperature contour at horizontal plane (ZX) at Y=0.9 m (head level)

Figure 5 shows the temperature distribution around the passengers' heads in Case 1. The simulations show that the temperature becomes approximately 26-30 degree Celsius around the heads of the driver and the front passenger, while it becomes approximately 26-28 degree Celsius around the rear passengers' heads. *Figure 6* shows the temperature distribution around the passengers' heads in Case 2, where the temperature becomes approximately 32-34 degree Celsius around the heads of the driver and the front passenger, while it becomes approximately 28-30 degree Celsius around the rear passengers' heads. The temperatures between the cabin side walls and the passengers are relatively high due to the skin temperature of the passengers and the effect of solar radiation [9].

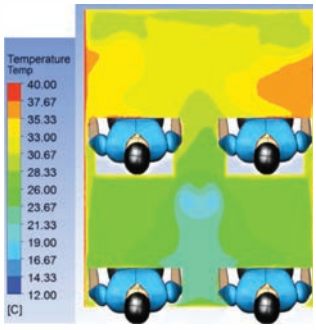

Figure 7: Temperature contour at horizontal plane (ZX) at Y=0.7 m (chest level)

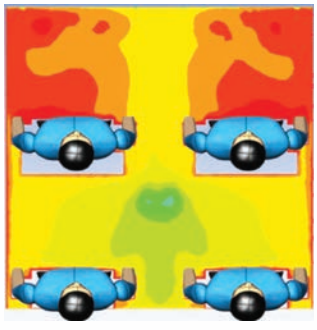

Figure 8: Temperature contour at horizontal plane (ZX) at Y=0.7 m (chest level)

Figure 7 shows that the temperature becomes approximately 30-34 degree Celsius around the chests of the driver and the front passenger in Case 1, while it becomes approximately 26-28 degree Celsius around the rear passengers' chests. *Figure 8* shows that the temperature becomes approximately 34-36 degree Celsius around the chests of the driver and the front passenger in Case 2, while it becomes approximately 30-32 degree Celsius around the rear passengers' chests.

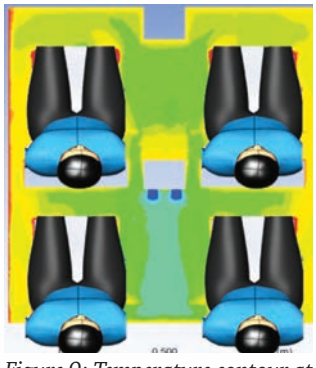

Figure 9: Temperature contour at horizontal plane (ZX) at Y=0.45 m (knee level)

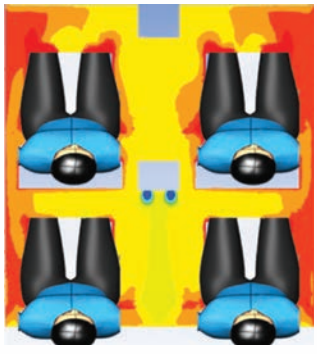

Figure 10: Temperature contour at horizontal plane (ZX) at Y=0.45 m (knee level)

Figure 9 shows that the temperature becomes approximately 26-30 degree Celsius around the knees of all passengers in Case 1. *Figure 10* shows that temperature becomes approximately 34-36 degree Celsius around the knees of all passengers in Case 2.

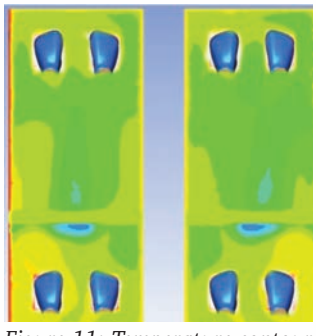

Figure 11: Temperature contour at horizontal plane (ZX) at Y=0.13 m (foot level)

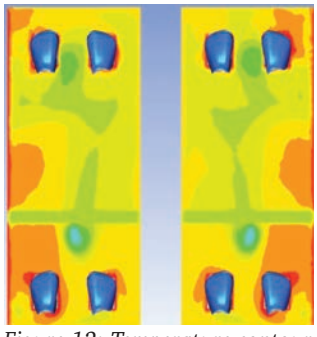

Figure 12: Temperature contour at horizontal plane (ZX) at Y=0.13 m (foot level)

Figure 11 shows that the temperature becomes approximately 26-28 degree Celsius around the feet of the driver and the front passenger in Case 1, while it becomes approximately 28-30 degree Celsius around the rear passengers' feet. *Figure 12* shows that the temperature becomes approximately 30-32 degree Celsius around the feet of the driver and the front passenger in Case 2, while it becomes approximately 32-34 degree Celsius around the rear passengers' feet [9].

Velocity Contours

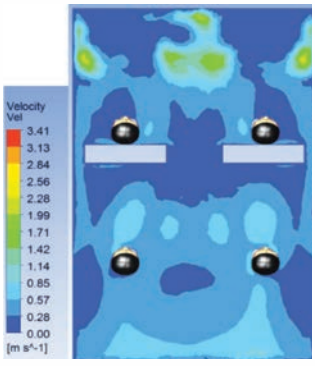

Figure 13: Velocity contour at horizontal plane (ZX) at Y=0.9 m (head level)

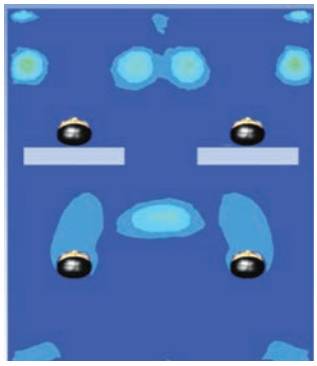

Figure 14: Velocity contour at horizontal plane (ZX) at Y=0.9 m (head level)

Figure 13 shows the velocity distribution around the passengers' heads in Case 1. The simulations show that the velocity becomes approximately 0.6 m/s around the heads of the driver and the front passenger, while it becomes approximately 0.7 m/s around the rear passengers' heads. *Figure 14* shows the velocity distribution around the passengers' heads in Case 2. The velocity becomes approximately 0.25 m/s around the heads of the driver and the front passenger, while it becomes approximately 0.5 m/s around the rear passengers' heads.

Figure 15: Velocity contour at horizontal plane (ZX) at Y=0.7 m (chest level)

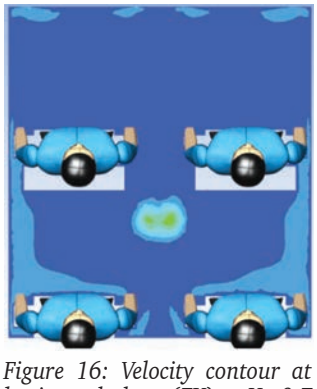

Figure 16: Velocity contour at horizontal plane (ZX) at Y=0.7 m (chest level)

Figure 15 shows that the velocity becomes approximately 0.3 m/s around the chests of the driver and the front passenger, while it becomes approximately 0.7 m/s around the rear passengers' chests. *Figure 16* shows that the velocity becomes approximately 0.25 m/s around the chests of the driver and the front passenger in Case 2, while it becomes approximately 0.5 m/s around the rear passengers' chests.

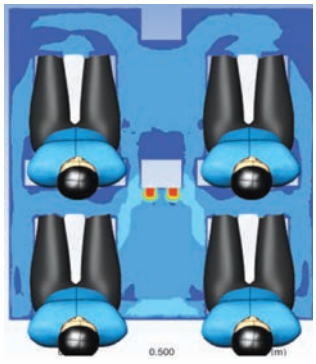

Figure 17: Velocity contour at horizontal plane (ZX) at Y=0.45 m (knee level)

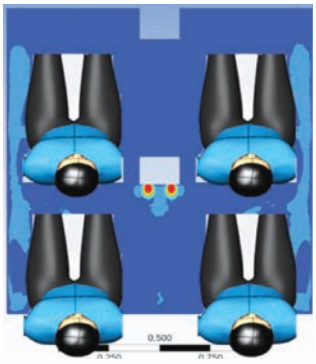

Figure 18: Velocity contour at horizontal plane (ZX) at Y=0.45 m (knee level)

Figure 17 shows that the velocity becomes approximately 0.7 m/s around the knees of all the passengers in Case 1. *Figure 18* shows that the velocity becomes approximately 0.25 m/s around the knees of the driver and the front passenger in Case 2, while it becomes approximately 0.5 m/s around the rear passengers' knees.

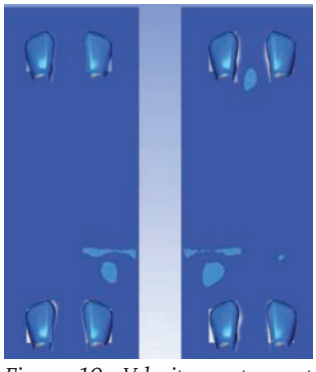

Figure 19: Velocity contour at horizontal plane (ZX) at Y=0.13 m (foot level)

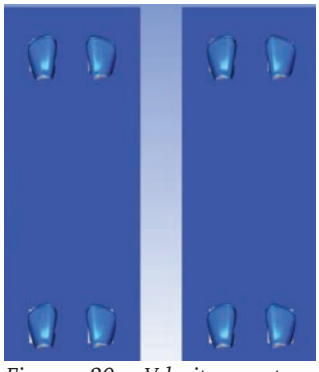

Figure 20: Velocity contour at horizontal plane (ZX) at Y=0.13 m (foot level)

Figure 19 and *20* show that the velocity becomes approximately 0.25 m/s around the feet of all passengers in Case 1 as well as Case 2.

Relative Humidity Contour

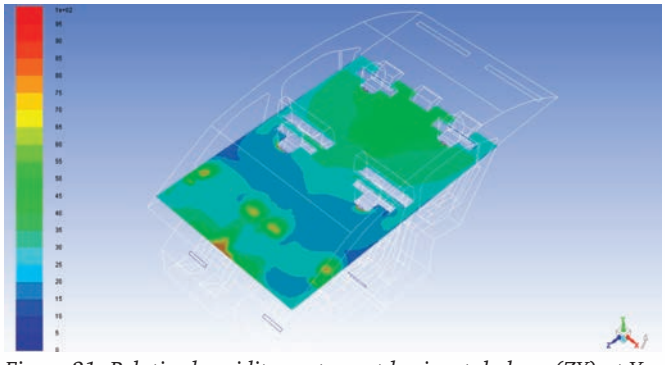

Figure 21: Relative humidity contour at horizontal plane (ZX) at Y= 0.83 m (mouth level) in Case 1

Figure 21 shows the relative humidity distribution inside the cabin at mouth level in Case 1. The simulations show that

relative humidity reaches 30% in the first half of the cabin, while it becomes approximately 45% in the second half. Solar radiation effect appears near the sides of the cabin and windshield, where relative humidity is around 5% [9].

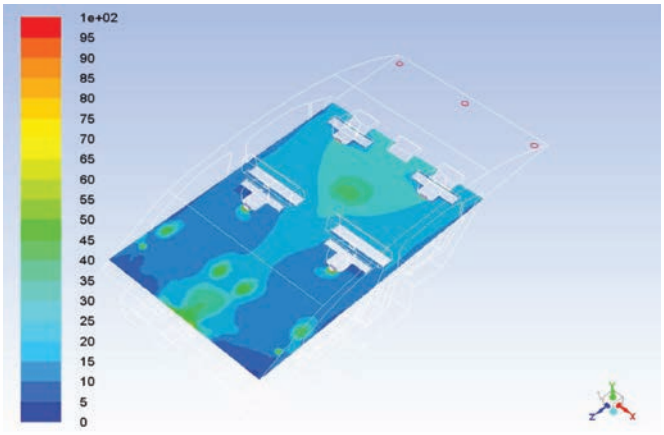

Figure 22: Relative humidity contour at horizontal plane (ZX) at Y= 0.83 m (mouth level) in Case 2

Figure 22 shows the relative humidity distribution inside the cabin at mouth level in Case 2. The simulations show that relative humidity reaches 10-20 % in the first half of the cabin, while it becomes approximately 25-35% in the second half. These values reflect the adverse relative humidity distribution due to relatively high temperatures.

PMV and PPD Contours

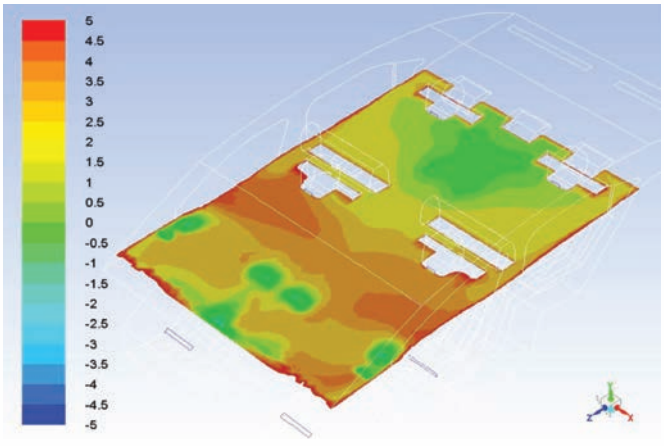

Figure 23: PMV contour at horizontal plane (ZX) at Y= 0.83 m (mouth level) in Case 1

Figure 23 shows the PMV contour inside the cabin at mouth level in Case 1. The simulations show a bad distribution ('too hot' may reach +3) in the whole cabin except the middle of the cabin in the second half and near the air inlets in the first half of the cabin, where its value is between -0.5 and +0.5.

Figure 24 shows the PPD contour inside the cabin at mouth level in Case 1. The simulations show a bad distribution with nearly 100% dissatisfaction, especially in the left and right sides of the cabin and near the windshield, due to the effect of solar radiation. The PPD values are affected by the PMV values because

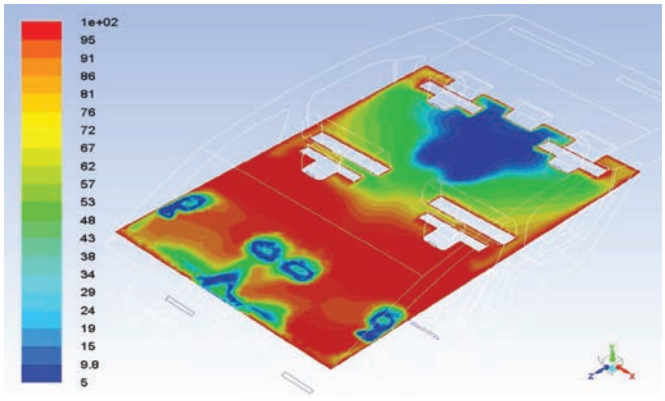

Figure 24: PPD contour at horizontal plane (ZX) at Y= 0.83 m (mouth level) in Case 1

the PPD equation is a function of the PMV. The PPD values around the heads of the driver and front passenger are nearly 100%, and around the rear passengers' heads about 50%.

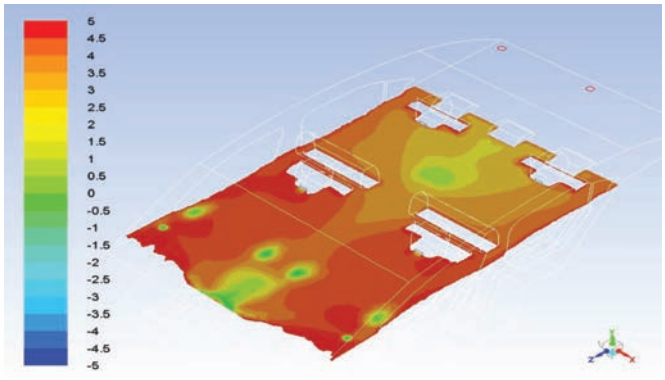

Figure 25: PMV contour at horizontal plane (ZX) at Y= 0.83 m (mouth level) in Case 2

Figure 25 shows the PMV contour inside the cabin at mouth level in Case 2. The simulations show a bad distribution ('too hot' may reach +3) in the whole cabin except the middle of the cabin in the second half and near the air inlets in the first half of the cabin, where its value is between -0.5 and +0.5.

Figure 26 shows the PPD contour inside the cabin at mouth level in Case 2. The simulations show a bad distribution near 100% dissatisfaction, especially in the left and right sides of the cabin and

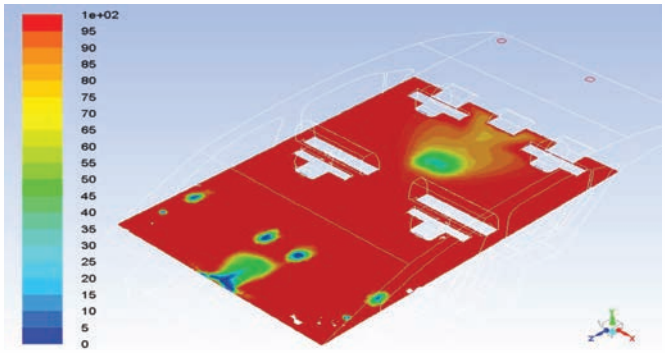

Figure 26: PPD contour at horizontal plane (ZX) at Y= 0.83 m (mouth level)

near the windshield due to the effect of solar radiation [9]. The PPD values are affected by the PMV values because the PPD equation is a function of the PMV. The PPD values around the heads of the driver and the front passenger are about 100% and around the rear passengers' heads about 50%.

Concluding Remarks

According to the results found in the above comparison obtained by using numerical investigation, the following conclusions can be expressed:

- The airflow regimes obtained by the configuration in Case 1, which has rectangular outlets, is better than the circular outlets in the Case 2 configuration.
- The rectangular shape of air terminals in vehicular HVAC systems gives temperatures lower by 2-4°C when compared with the circular shape, while the velocity in circular outlets is lower than rectangular outlets.
- Both the configurations achieve bad agreement between the average air velocity and average temperature with ASHRAE comfort conditions. Within the occupied zones, the temperature inside the cabin exceeds 26°C, relative humidity is lower than 50% in the whole cabin, air velocity is higher than 0.25 m/s, PMV contour inside the whole cabin is about +3 satisfaction which means 'too hot' feeling leading to discomfort, and PPD may reach 100% dissatisfaction in a major area inside the cabin.

References

L. D. Frank, M. A. Andresen and T. L. Schmidt, "Obesity relationships with community design, physical activity, and time spent in cars", Am. J. Prev. Med., vol. 27, no. 2, pp. 87–96, Aug. 2004;

ASHRAE, "Thermal environmental conditions for human occupancy", ANSI/ASHRAE Standard 55-2013, American Society of Heating, Refrigerating and Air-Conditioning Engineers, Atlanta, GA, in, 2013.

Miloš Fojtlín, A, Michal Planka, Jan Fišer, Jan Pokorný and Miroslav Jícha, "Airflow Measurement of the Car HVAC Unit Using Hot-wire Anemometry", EPJ web of conferences 114,02023-2016.

Joo Hyun Moon, Jin Woon Lee, Chan Ho Jeong, Seong Hyuk Lee, "Thermal comfort analysis in a passenger compartment considering the solar radiation effect", International Journal of Thermal Sciences 107, 77e88-2016.

Han T, Huang L., "A model relating a thermal comfort scale to EHT comfort index", SAE Technical Paper, 2004, p. 01e0919.

Fluke 561 Infrared Thermometer User Manual, USA, Fluke Corporation; 2006.

Mezrhab A, Bouzidi M., "Computation of thermal comfort inside a passenger car compartment", Applied Thermal Engg., 2006; 26:1697e704.

Adhikari VP, Nassar A, Nagpurwala QH, "Numerical studies on the effect of cooling vent setting and solar radiation on air flow and temperature distribution in a passenger car", SAE Technical Paper, p. 28e0048.2009.

I. Reda, "Air Flow Regimes and Thermal Comfort In Vehicle Cabin Considering Solar Radiation", MSc, Cairo University, July 2017.